Final Report

Kimberly Anderson (PI)
University of Minnesota
Minneapolis, MN 55455
T: 612-624-2316
And06109@umn.edu

Project Title: Development of a Real-time Inhalable Particle Spectrometer

Project Dates: 9/1/2015 – 8/31/2018

NIOSH Grant #: 6 K01OH010763-01

Report Date: 11/26/19

Table of Contents

Abstract

Particle sizes 20 μm and larger exist in the workplace and can constitute as much as 50% or more of the inhaled dose to workers. However, instruments capable of measuring particle sizes between 20 and 100 μm are limited. For the purpose of exposure assessment, NIOSH currently specifies the 37-mm cassette, a time-integrated, mass-based method, for the measurement of inhalable particles in the workplace; this device has been shown to under-sample particles between 20 and 100 μm in size. Other inhalable samplers exist (IOM and Button sampler), but those too are mass-based instruments. Such filter-based instruments, while useful for assessing personal exposure, provide no information on the particle size distribution. All of these methods collect samples over an 8-hour period, thus temporal and spatial information on the aerosol hazard is lost. Large particles settle out quickly in air (terminal settling velocity of 100 μm particle = 0.3 m/s). Because these aerosol hazards are short-lived, a time-integrated measurement may not accurately capture these exposures. In such cases, a time-resolved instrument is required to capture the timing and magnitude of exposure. Time-resolved instruments currently exist to characterize the size distribution of aerosols in the range of 0.05 to 20 μm. There are limited time-resolved (or even time-integrated) devices that are capable of measuring the size distribution (and concentration) of particles from 20 to 100 μm.
Exposure and particle deposition in the respiratory system is largely governed by particle size. There is size-dependent deposition in the head airways for particles from 10 to 50 μm. Particles 30 μm and larger are more likely to deposit in the oral cavity while 10 μm particles have the highest deposition in the tracheobronchial region. Exposure to large inhalable particles can deliver massive doses to workers and contribute substantially to the inhaled dose. For example, the mass of one 100 μm particle would be equivalent to the mass of one million 1 μm particles of equal shape/composition. Data on the burden of disease from occupational aerosol exposures shows evidence of symptomatic health effects resulting from exposure to large particles in numerous workplaces. Studies show occupational rhinitis (acute or chronic), chronic pharyngitis, chronic sinusitis, nasal cancer, chronic laryngitis and gastro-intestinal diseases occurring in many industries, which would indicate the presence of particles 30 μm and larger (because such particles are more likely to deposit in the head airways). However, we lack the tools to characterize such hazards quantitatively. This project developed a new instrument to characterize the size distribution of inhalable particles in the workplace and developed an optical detection for real-time measurement of particle size and concentration.

Section 1

Significant (Key) Findings.

Key Finding #1: The virtual impactor/colliding flow principles were capable of size-separating large inhalable particles. This research lead to the development of a sampler can be used to improve exposure assessment methods in industries where large inhalable particles pose a hazard.

Key Finding #2: Mie scattering system can be used to detect particles 13-96.5 μm in real-time. This system will allow researchers to make fast, accurate measurements of aerosol size distributions between 20 and 100 μm.

Translation of Findings.

The development of the vPIPS sampler and optical detection system are capable of characterizing the size-distribution of inhalable particles in the workplace, giving industrial hygienists and exposure scientists a tool to evaluate a hazard that has been difficult to quantify.

Outcomes/Impacts.

This project developed a sampler capable of size-segregating large (10-100 μm) particles and developed an optical detection system. A real-time spectrometer would be useful in situations where aerosol hazards have bimodal size distributions, such as in the paper, wood and thermoplastic industries which all showed bimodal, log-normal particle distributions with the mass median aerodynamic mean in the range of 40 to 60 μm and allow for the evaluation of hazards that have not been quantified. Once this instrument is commercialized, it will enable occupational health professionals to assess inhalable aerosol hazards more fully, as no commercially-available technologies currently exist to meet this need. This instrument will enable more accurate assessment of worker exposure, better selection of control methods, and improved understanding of the target organs/regions of effect from inhalable aerosol exposure (as particle size governs deposition/fate in the body). The results from this study were used as preliminary data for an R21 proposal adding laser induced breakdown spectroscopy to the inhalable particle sizer.

Section II. Scientific Report

Particle size is important parameter to predict deposition in the human respiratory system and consequently adverse health effects due to aerosol exposure. In order to accurately assess exposure and health effects knowledge of the particle size is crucial. A real-time spectrometer would be useful in situations where aerosol hazards have bimodal size distributions, such as in the paper, wood and thermoplastic industries which all showed bimodal, log-normal particle distributions with the mass median aerodynamic mean in the range of 40 to 60 μm. For example, in the woodworking industry most wood dust particles have sizes larger than 10 μm and have bimodal size distributions. This bimodal distribution causes very different health effects associated with exposure to different particle sizes.

The goal of this project was to develop a time-resolved spectrometer to characterize the size distribution of inhalable particles in the workplace. Our approach was to use the principles of virtual impaction combined with vertical elutriation to separate large particles from quiescent air as a function of aerodynamic diameter and develop and incorporate an optical detection system based on Mie scattering principles for the real-time detection of aerosols as they passed through the detection region. During this project, we achieved this aim and demonstrated feasibility of the optical detection system. This project had three specific aims; progress for each aim is discussed below.

Aim 1a: Optimize the design of a portable inhalable particle spectrometer (PIPS) to segregate inhalable aerosols as a function of particle size.

<u>CFD Modeling:</u> In the first year of this project, computational fluid dynamics (CFD) modeling was conducted to determine the optimal inlet size and separation distance. Simulations evaluated three inlet opening sizes (15, 20, 35 mm) and two separation distances (10 and 15 mm). Simulations were conducted for all three inlet opening sizes and separation distances for the 50 μm cutoff for a total of six simulations. Sampling efficiency for inlet opening sizes of 15 and 20 mm showed little differences (Figure 1). An inlet opening size of 35 mm resulted in a less sharp cutoff curve.

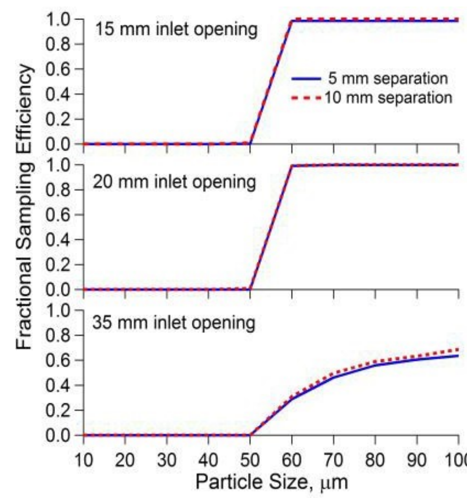

Figure 1: Effect of inlet diameter and separation distance on sampling efficiency.

Separation distance did not affect the sampling efficiency curves. Based on these results, inlet openings of 15 and 20 mm and separation distances of 10 and 5 mm were used for the remaining simulations.

Sampling efficiency was simulated for six cutoff curves (30, 40, 50, 60, 70, and 80 μm), two inlet diameters (15 and 20 mm), and two separation distances (5 and 10 mm) for a total of 24 simulations. Particle deposition on the interior sampler walls was found to be minimal (<5%).

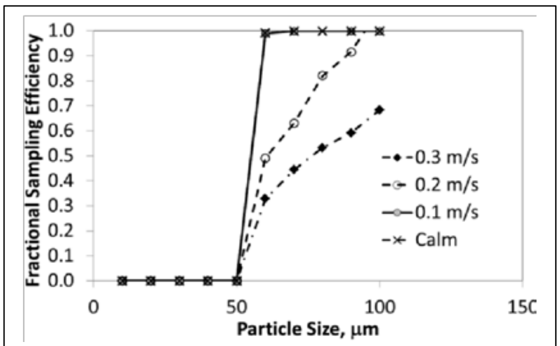

Figure 2: Effect of increasing wind speed on sampling efficiency. Data is for the 50 μm cut

The effect of ambient wind speed on sampling efficiency was investigated for the 50 μm cutoff size (Figure 2). Three wind speeds were simulated: 0.1, 0.2, and 0.3 m/s. At 0.1 m/s, the sampling efficiency was the same as for calm air. At 0.2 and 0.3 m/s the sampling efficiency curves became less steep and overall sampling efficiency dropped below 100% for particles larger than the cut size.

Prototype Sampler: A prototype sampler (Figure 3) based on the design identified in the CFD models was built. Caps with inlet diameters of 15 and 20 mm and separation distances of 5 and 10 mm, were machined. Holes were drilled out and tapped to incorporate lasers and detectors for real-time counting.

The prototype sampler was fitted with a 785 nm 100 mW laser diode (L785P090, Thorlabs, Newton NY, USA) and Si photodiode detector (FDS100, Thorlabs, Newton NY, USA). A Labview data acquisition card was used to monitor the signal from the detector. Several different optical detection configurations were evaluated including a 2 mm laser beam, a laser sheet with a 25° divergence angle with detectors at 30, 60, and 75°.

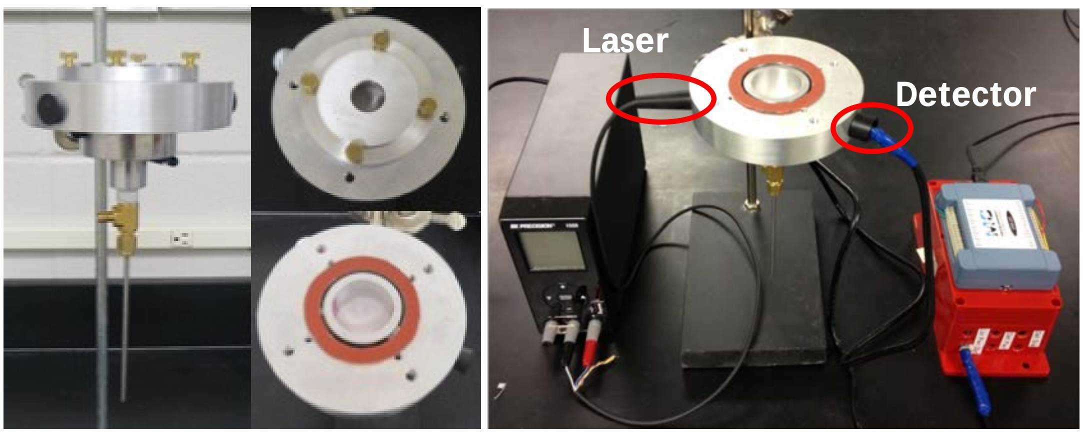

Figure 3: Prototype sampler and proof-of-concept optical detection system.

The original optical detection system design used a laser beam and detector at a 20° scattering angle and a 4mm^2 detection region. While this setup was able to detect particles as they passed through the detection region, particle counts were very low (<1% compared to particles counted on the filter), due to the small detection region of the optical setup. Thus, a negative concave lens was used to spread the laser beam into a sheet to increase the size of the particle detection region by 12-fold. The new laser sheet configuration required the detector to be placed at a minimum of 30° scattering angle in order to avoid light scattering directly into the detector.

Development of the Particle Scattering Model

Although the laser sheet increased the detection region, the laser intensity decreased as a result. We developed a theoretical modeling framework using Mie theory that predicts particle scattering within a two-dimensional 'laser sheet' within the cross-section of the PIPS detection region in order to evaluate if the predicted particle signals would be high enough above background noise to detect particles. The mathematical model also allowed us to optimize the size of the laser sheet and detector orientation to maximize particle signals.

Particle Scattering Model

Particle distance to the detector lens, kd, was calculated for all positions across the pips cup using equation 1:

$$k_D = \sqrt{(x_D - x)^2 + (y_D - y)^2 + (z_D - z)^2} \quad (1)$$

where x_D, y_D, and z_D are the coordinates of the detector center with respect to the center of the PIPS sampler.

Particle distance to the laser, k_L (m) was calculated using

$$k_L = \sqrt{(x_L - x)^2 + (y_L - y)^2 + (z_L - z)^2} \quad (2)$$

where x_L, y_L, and z_L are the coordinates to the center of the laser beam with respect to the center of the PIPS sampler.

Particle scattering angle to the detector was calculated using

$$\alpha = \arctan\left(\frac{y_D - y}{x_D - x}\right) \quad (3)$$

Mie scattering of the particle as a function of scattering angle (eq 3) is computed using Matlab code. The Mie scattering is a function of particle size, refractive index (which depends on particle composition). Q_{scat} is the mie scattering efficiency normalized to the particle crosssection. C_{scat} is the scattering cross-sectional area. Q_{scat} was obtained from Matzler's Matlab code. C_{sca} was computed:

$$C_{sca} = Q_{sca} * \pi * r^2 \quad (4)$$

Phase functions were obtained from MiePlot for polystyrene particles at 785 nm. The differential scattering cross section is the angular distribution of the scattered light (the amount of light scattered into a unit solid angle about a given direction).

Differential scattering cross sections, :<; were calculated by multiplying the phase function by Csa/4π.

The area of the laser was calculated using equation 5:

$$A_{Laser} = \sqrt{x^2 + y^2} * b * 2\beta \quad (5)$$

Where β = sheet half angle (angle of laser spreading)

$$\beta = 12.5 * \left(\frac{\pi}{180}\right)$$

And b is the laser sheet thickness b = 2 mm.

Laser intensity as a function of position in the laser sheet was calculated using equation 6:

$I(x, y) =$ 4 $(8R78)ST->(5R?@A75 / 0PQ@A)ST(UR7U)S9*V*)W (6)

where the laser power was set at 0.09 W.

Scattered power as a function of position in the laser sheet was computed using equation 7:

$$Scattered \quad Power \; (x, y) = \frac{\partial\sigma}{\partial\Omega}(\alpha) * I_{b>?@A(8,5)} * \Omega_{8,5} \tag{7}$$

Where $\Omega(x, y)$ is the solid angle for each position in steradians, calculated by:

$$\Omega(x, y) = \frac{d" \, S}{\frac{L}{2}} * 4_{edf6} \quad \pi \tag{8}$$

And where D_L is the diameter of the lens, 0.5 inches (0.0127 m).
Predicted voltage as a function of position was computed using:

$$Predicted \quad Detector \quad Voltage \quad (x, y) = Scattered \quad power * Detector \quad Response \tag{9}$$

Where the detector response is 0.025 V/µW at a detector gain of 1.

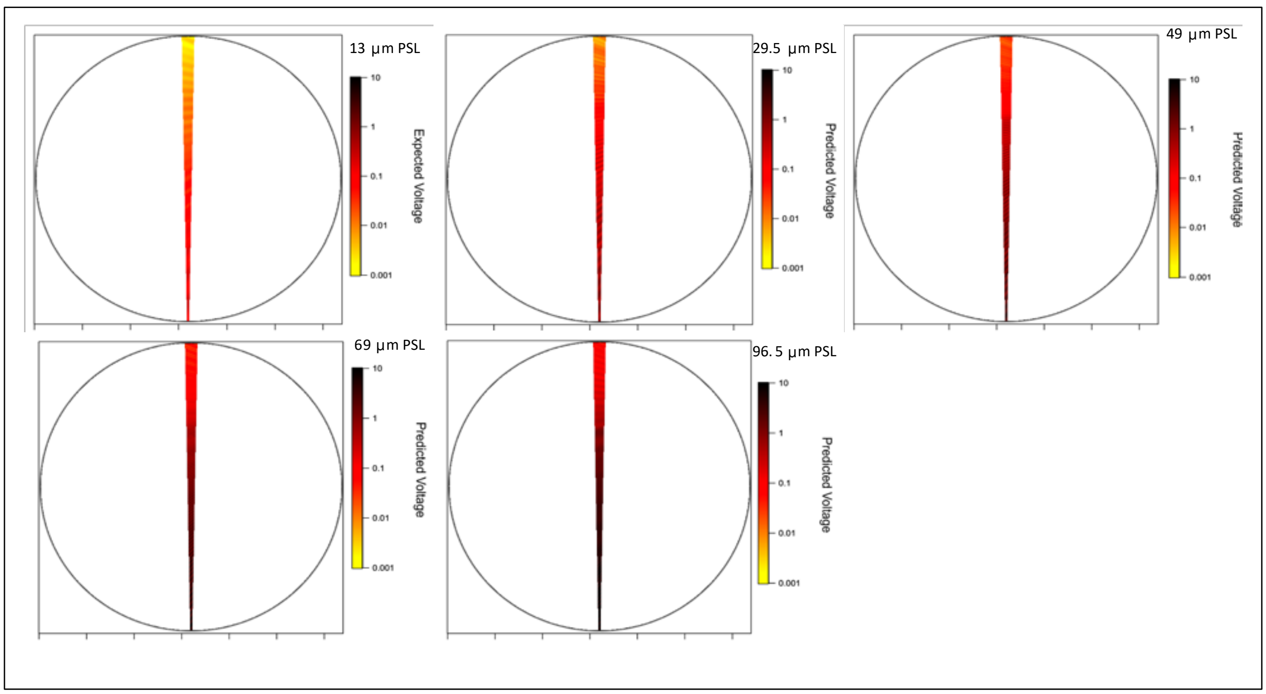

Figure 4: Modeled signal for PSL spheres from 13-96.5 µm.

Several configurations of the position of the laser beam and detector were evaluated to determine the optimal design for maximum signal strength while minimizing the noise.

First, a laser beam with a 2 mm width was evaluated for polystyrene fluorescent spheres with diameters of 13, 29.5, 49, 69 and 96.5 mm was modeled. Next, we modeled the predicted signal when the laser beam was spread out into a laser sheet at a 25-degree divergence angle. We evaluated three detector orientations for the laser sheet: 30, 60, and 75°.

For the laser beam, signals ranged from 0.02 to 5 volts (Figure 4).
Below 0.02 volts, signals from the light scattering on the particles cannot be detected above the background noise of the optical detection system. The intensity of the laser decreases as the beam was spread out into a sheet, resulting in a reduction in the predicted signal (Figure 5). For the 13 µm particles, the average signal in the detection region decreased from 0.0263 volts for the laser beam to 0.017 volts for the laser sheet with the detector at 30°. As the detector was rotated away from the forward scattering direction, signal strength substantially decreased for all particle sizes. For the 13 um particles, predicted signals for the laser sheet for all detector orientations were below the limit of detection. However, the laser sheet for particles >13 µm was able to differentiate the signals from particle light scattering.

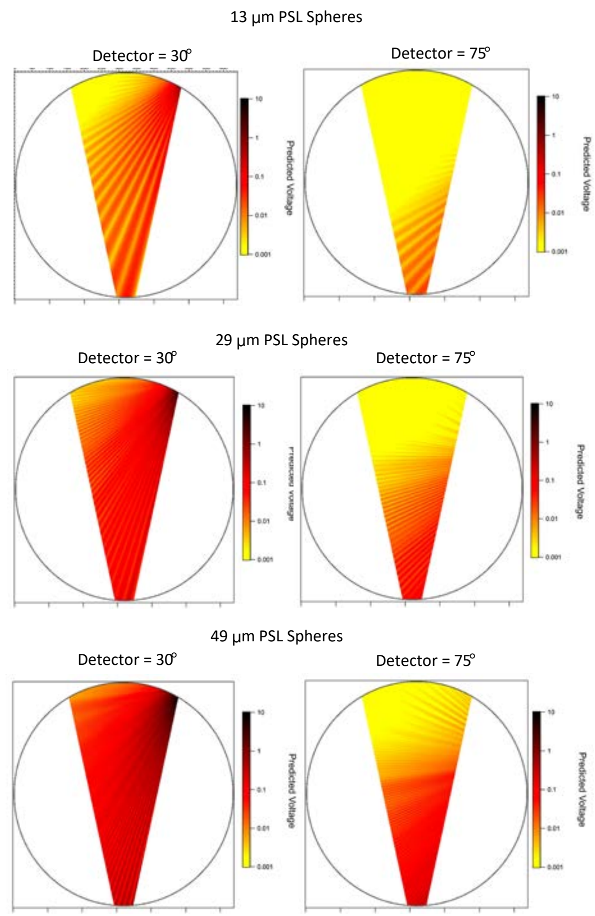

Figure 6: Predicted Signals for 13, 29.5, and 49-µm particles. Regions in yellow are below the limit of detection.

Aim 1b – Develop a transfer function to convert measurement data into airborne particle size distribution.

A data inversion was developed to estimate a continuous size distribution from measured particle counts in discrete bins. A logistic function was fitted to the sampling efficiency curves for each cut point. The coefficients were obtained by nonlinear, least-squares regression. Next, an initial approximation of a count median diameter (CMD) of 52 µm and standard deviation (SD) of 15 µm were used as a random starting point; these CMD and SD values were then adjusted through a series of iterations to arrive at the optimal solution. A data-inversion spreadsheet was developed in Microsoft Excel (2010, Microsoft Corp., Seattle, WA) to estimate the CMD, SD, and number concentration of a normally distributed, unimodal aerosol from particle number concentrations measured with the vPIPS sampler at six cutpoints following the method described by O'Shaughnessy and Raabe (O'Shaughnessy and Raabe 2003). The data inversion procedure worked reasonably well (Figure 7), although the it slightly overestimated the count median diameter.

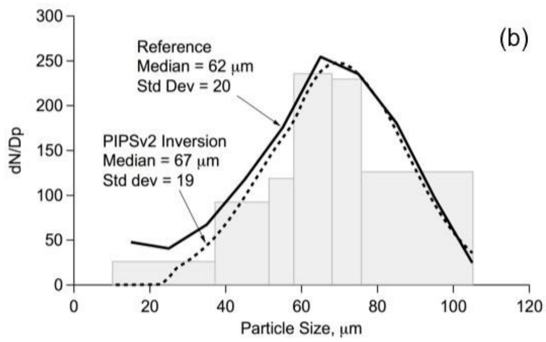

Figure 7: PIPSv2 size distribution using data inversion procedure

Aim 2 – Evaluate the performance of the real-time particle spectrometer in the laboratory Aim 2 tested the sampler in the calm air chamber. Filters were placed in the bottom of the collection tube and in reference samplers located in the testing section of the calm air chamber. Sampling efficiency for each cut size (30, 40, 50, 60, 70, and 80 µm) was measured. The polydisperse test powder was fluorescent, polyethylene microspheres of unit density with sizes ranging from 10 to 90 µm (UVYGPMS, Cospheric LLC). An epi-fluorescent microscope (Orthoplan, Leica) and fluorescence filters (Vivid Plus Set XF05-2/B, Omega Optical) were used to image collected particles. Filters were imaged under a 1.6x objective lens and a 10x objective eyepiece. ImageJ software (NIH, V1.46r (Rasband)) was used to obtain the area of each particle, from which the corresponding particle aerodynamic diameters were calculated using Microsoft Excel. A stage micrometer provided a reference for ImageJ size analysis. Size distributions of the reference samplers were measured using microscopic analysis following the procedure outlined above. Particles were sorted by aerodynamic diameter into one of nine size bins from 15 to 95 µm, each with a 10-µm bin width.

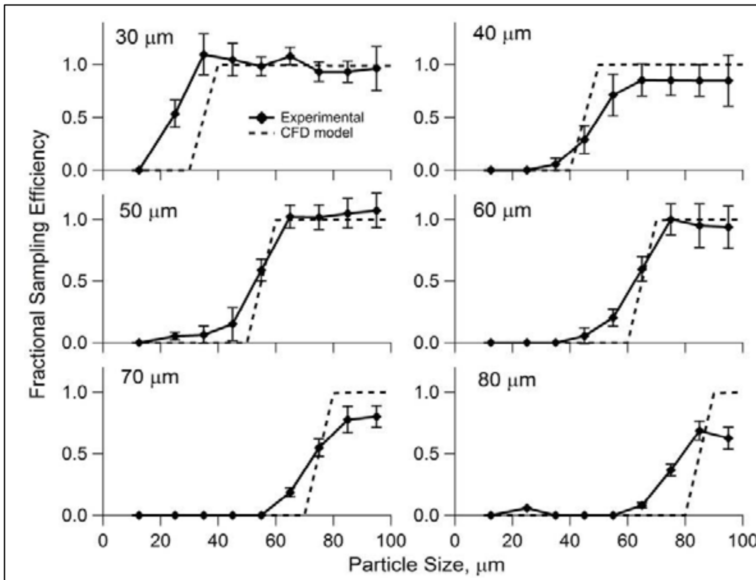

Figure 8: Sampling efficiency curves for vPIPS sampler

The experimental and simulated sampling efficiency curves at the six cut points for the sampler are displayed in Figure 8. The error bars in this figure represent one standard deviation based on the variability between sampling efficiency measurements for repeated experiments. The sampler was designed to minimize the jet effect at the top of the collection tube while maintaining a flat velocity profile throughout the tube. Experimental sampling efficiency for the sampler compared reasonably well to CFD simulations (Figure 8). The 70 and 80 μm cuts had the greatest differences between experimental and simulated efficiencies, with experiments underestimating simulated sampling efficiencies by 20 to 30% for particles larger than the cut size. These sampling efficiency curves are based on particle counts measured on the filter at the base of the collection tube.

Experimental Testing to Validate the Theoretical Mie Scattering Model

Experimental tests using narrowly dispersed polystyrene particles were conducted in a calm air chamber to validate the theoretical modeling. A vertical, calm air chamber (1.5 m high with 0.9 m x 0.9 m cross section) was designed and built to evaluate the detector efficiency. Particles were aspirated into the upper section of the chamber and settled into the testing section of the chamber. The aerosol dispersion system consisted of a holder where the dust was deposited which was connected to a compressed air line. A solenoid valve separated the dust holder from the compressed air line. When the solenoid valve was activated, a jet of air ejected the test aerosol into the chamber. For each test, the solenoid valve was activated once for less than 5 seconds. A honeycomb diffusion screen (25 mm opening size) was located below the aerosol dispersion system (at a height of 0.9 m) to minimize any turbulent eddies generated by the aerosol dispersion system. The test aerosol was allowed to settle for 10 minutes, which was more than sufficient time for the smallest particle size to settle to the base of the chamber. Aerosol dispersion in the testing section of the chamber was found to be uniform, with no significant differences in number concentration or count median diameter between locations.

Fluorescent, polyethylene microspheres of unit density with narrowly distributed sizes were used as the test aerosol. Four particle sizes were used to test the detector performance: 27-32, 45-53, 63-75, and 90-106 μm. An epifluorescent microscope (Olympus) and fluorescence filters (PLAPON2X, Olympus) were used to image particles collected on the filters. Filters were imaged under a 2x objective lens. ImageJ software (NIH, V1.46r [Rasband]) was used to obtain the area of each particle, from which the corresponding particle equivalent diameters were calculated using Microsoft Excel. A stage micrometer provided a reference for ImageJ size analysis.

Particle counts in the detection region were measured using a DAQ card and the signal processed using a Labview program and IgorPro. Voltage measured by the detection system were compared to predicted voltage from the mathematical model.

Measured and modeled signals agreed reasonably well (Figure 9). The Mie scattering model did reasonably well at predicting the signal for particles less than 49 µm. However, for particles larger than 49 µm, the model overestimated the signal. As particle size increased, the signal became more variable due to the varying intensity of the laser sheet cross section and the position of the particle within the sheet. Reduction of stray scatter light was found to be critical to enable detection of the needed signals.

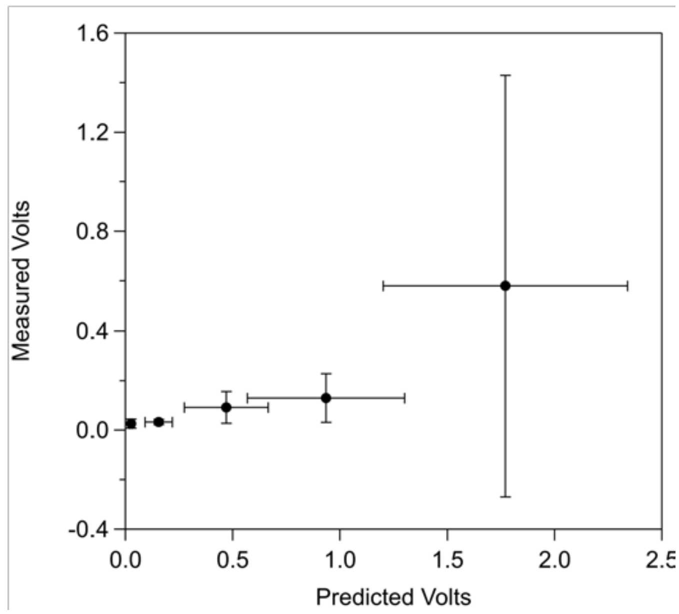

Figure 9: Measured versus predicted signals for PSL spheres of 13, 29.5, 49, 69, and 96.5 µm

This project developed a sampler that could be beneficial to exposure assessment scientists and industrial hygienists. Until now, it has been difficult to quantify hazards associated with exposure to large, inhalable particles due to a lack of measurement technology. We have developed a real-time optical detection system for this sampler, which expands the usefulness, as large inhalable particles settle quickly through air. This sampler could be used to determine size distribution of aerosols as a function of job task or to evaluate how aerosol size distribution changes over time.

Published Papers

Anderson KR, D Leith, M Ndonga and J Volckens. (2015) Novel Instrument to Separate Large Inhalable Particles. Aerosol Science and Technology, 49(12): 1195-1209, DOI: 10.1080/02786826.2015.1112874

Conference Presentations

Kimberly Anderson, Sean Walsh, Azer Yalin, John Volckens, "Design and Optimization of an Optical Detector for the Portable Inhalable Particle Sizer," oral presentation, American Association of Aerosol Research (AAAR), Minneapolis, MN, October 2015.

Kimberly Anderson, Dave Leith, Sean Walsh, Jordan Rath, Azer Yalin, John Volckens, "Design and experimental testing of an inhalable particle spectrometer," oral presentation, American Association of Aerosol Research (AAAR), Orlando, FL, October 2014.

Project Outcomes

"Portable Particle Spectrometer." Volckens, J., Anderson, K.R., et al. Filed by Colorado State University Research Foundation on 10/26/2015; #62/066,64